

# A laser-deposition approach to compositional-spread discovery of materials on conventional sample sizes

Hans M Christen, Isao Ohkubo, Christopher M Rouleau, Gerald E Jellison Jr, Alex A Puretzky, David B Geohegan and Douglas H Lowndes

Oak Ridge National Laboratory, PO Box 2008, Oak Ridge, TN 37831-6056, USA

E-mail: christenhm@ornl.gov

Received 14 April 2004, in final form 10 August 2004

Published 16 December 2004

Online at [stacks.iop.org/MST/16/21](http://stacks.iop.org/MST/16/21)

## Abstract

Parallel (multi-sample) approaches, such as discrete combinatorial synthesis or continuous compositional-spread (CCS), can significantly increase the rate of materials discovery and process optimization. Here we review our generalized CCS method, based on pulsed-laser deposition, in which the synchronization between laser firing and substrate translation (behind a fixed slit aperture) yields the desired variations of composition and thickness. *In situ* alloying makes this approach applicable to the non-equilibrium synthesis of metastable phases. Deposition on a heater plate with a controlled spatial temperature variation can additionally be used for growth-temperature-dependence studies. Composition and temperature variations are controlled on length scales large enough to yield sample sizes sufficient for conventional characterization techniques (such as temperature-dependent measurements of resistivity or magnetic properties). This technique has been applied to various experimental studies, and we present here the results for the growth of electro-optic materials ( $\text{Sr}_x\text{Ba}_{1-x}\text{Nb}_2\text{O}_6$ ) and magnetic perovskites ( $\text{Sr}_{1-x}\text{Ca}_x\text{RuO}_3$ ), and discuss the application to the understanding and optimization of catalysts used in the synthesis of dense forests of carbon nanotubes.

**Keywords:** combinatorial materials synthesis, continuous compositional spread, thin films, pulsed-laser deposition

## Introduction

Recent years have brought great prominence to the field of combinatorial materials synthesis, inspired in large part by the success of related approaches in the chemical and pharmaceutical industries. Unfortunately, similar breakthroughs in thin-film research are still rare, at least in part because of the incredible technical challenges involved in the characterization of the produced materials. In this paper, we describe our approach and review representative results for a parallel multi-sample synthesis approach yielding a smaller number of samples but with sizes sufficient for traditional characterization techniques, therefore offering great potential as part of an integrated research effort.

Multi-sample approaches in thin-film research can be divided into two classes—the discrete combinatorial synthesis (DCS) (where individual ‘pixels’ of a substrate are coated with a film of predetermined composition) and the continuous compositional-spread (CCS) techniques.

Continuous compositional-spread approaches to thin-film synthesis are much older than these combinatorial approaches. Going beyond the study of chemical composition, the basic idea behind a ‘generalized’ CCS method is the possibility to simultaneously study the combined effect of two parameters, which are imposed as spatial variations along two different orientations of a planar substrate. Possible parameters are chemical composition, film thickness, growth temperature and their combinations. In 1965, Kennedy [1] introduced an

approach based on sputtering in which the key concepts of CCS and its generalization to growth-temperature optimization have been demonstrated. In that study, the simultaneous deposition of materials was shown to result in the formation of non-equilibrium intermetallic phases, and a temperature gradient across the substrate was imposed to study the effect of growth temperature on Ca–Mn alloys.

Further early successes of such CCS methods came from the optimization of growth parameters to obtain the desired film composition [2] or to form theoretically predicted materials (leading, for example, to the superconductor with the highest transition temperature known at that time [3]).

Sputter-based CCS methods have regained popularity with the widespread availability of electronic data analysis, and have been applied more recently to high- $k$  dielectrics [4] and transparent conducting oxides [5, 6]. Pulsed-laser deposition (PLD) has also been employed for such studies, either by the spatial overlap of two deposition plumes [4] or by the motion of a substrate between different deposition regions [7, 8]. The motivation for using PLD is obviously given by the technique's proven track record in the rapid prototyping and the synthesis of complex oxides.

One of the main difficulties encountered in these 'maskless' approaches is the inherently nonlinear spatial variation of the composition, and the simultaneous variations in film thickness. However, two developments have aided the perfection of CCS approaches. First, automation very similar to that used in DCS has become readily available and can be used to continuously move masks. The application of this technique in a precursor-based approach is straightforward [9–11]; unfortunately, the approach is only applicable to materials systems that can be synthesized in an equilibrium process.

The second key development is the realization that pulsed-laser deposition (PLD) can be used to obtain complex metastable alloys by the sequential deposition of sub-monolayer amounts of the individual constituents [12, 13]. This idea was originally applied to CCS in an approach in which the naturally occurring spatial growth-rate variations lead to intentional compositional changes across the sample [7], and later in combination with moving shields [14, 15].

Moving-shield approaches critically rely on the uniformity of the deposition zone across the entire substrate area, thus effectively limiting the compositional spread to an area of less than 2 cm in most cases. This may be desirable for approaches that are based on sophisticated analysis techniques such as scanning probes (scanning microwave microscopy [16], scanning SQUID microscopy [14]) or by careful simultaneous observation ('imaging') and analysis such as concurrent x-rays [14] or optical methods [9–11]. However, this size limitation seriously restricts the possibilities for characterization by conventional methods (SQUID magnetometry, resistance versus temperature measurements, etc), where each data point requires several square millimetres of thin-film material.

The approach reviewed in this paper addresses this issue by a moving-substrate (fixed mask) technique. For binary compositional spreads, the substrate size is thus only limited by the mechanical performance of the substrate holder/heater.

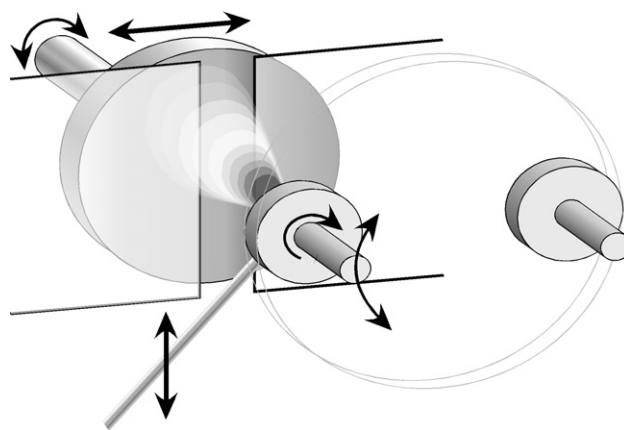


**Figure 1.** Schematic representation of the PLD system employed in this study. Arrows in the figure represent axes of motion that can be controlled and synchronized. Two targets are shown in the foreground, and the laser beam (entering from the lower left) impinges onto one of them, forming a plasma plume. This plume expands towards the substrate holder, shown behind the slit-shaped aperture.

Thus, this method provides a valuable alternative to the small-sample approaches, yielding samples that can be analysed by traditional measurement techniques.

Furthermore, a key benefit of the approach is the possibility to produce—with the identical equipment—uniform thin films of any of the compositions explored in a CCS experiment.

The paper is structured as follows: first, we describe our PLD apparatus and show how the synchronization between laser firing and substrate motion can be used to obtain uniform-thickness films. This principle is then applied to the uniform deposition on a row of samples that are placed on a substrate heater with a well-controlled lateral temperature variation, allowing for the rapid and systematic growth-temperature optimization. The laser/substrate synchronization approach is then applied to the growth of films with a controlled thickness variation, and we show as an application the optimization of catalysts for the long-length synthesis of carbon nanotubes (CNTs). Finally, the same basic principles are applied to true compositional spread and *in situ* alloy formation, with complex metal oxides given as an example.

### Synchronization between laser firing and target/substrate motion in PLD

The basic principles of PLD have been reviewed numerous times in the literature [17, 18]. The novel feature of the apparatus employed here is a precise and rapid synchronization between laser firing, substrate motion (translation and rotation) and target exchange. Figure 1 shows a schematic diagram of the system. Two (or more) targets can be rapidly positioned in the path of the focused laser beam, which impinges at an angle of  $45^\circ$ . The target–substrate distance in all experiments presented here was 6.5 cm. Laser-beam scanning is used to obtain more uniform target wear and to obtain a more uniform thickness distribution in the vertical direction. For larger areas, it would be possible to combine target motion with laser-beam scanning. As usual, each target additionally rotates around

its horizontal axis. A Lambda Physik LPX325i excimer laser with 248 nm radiation is used with an energy density per pulse of  $\sim 200$  mJ (for oxide targets) or 300 mJ (for metals) focused onto a spot measuring  $1 \text{ mm} \times 6 \text{ mm}$ . The advantage of using this 160 W laser is the option to run at high pulse repetition rates ( $>100$  Hz), which significantly increases deposition speed in approaches where a small amount of material must be deposited per pulse and substrate position in order to obtain the desired controlled profiles.

Deposition can occur through a slit-shaped aperture, defined by two independent and removable shields. Behind that aperture, the substrate heater can translate horizontally (travel range: 75 mm, positioning time:  $\leq 0.5$  s). When appropriate, this substrate plate can additionally be rotated continuously around its horizontal axis, or rapidly driven to any angular position.

Using this arrangement, and the electronic control of laser firing in synchrony with the mechanical motion of the components, a number of different ‘firing schemes’ can be designed, each with its specific advantages and applications.

## Growth of uniform films

### Uniform thickness on a large sample

While PLD has found most success in the growth of small samples of prototype materials, it is possible to uniformly coat a relatively large sample if the appropriate substrate translation and laser firing schemes are used.

Earlier work on uniform-film growth has relied on either an off-axis geometry (with the substrate positioned orthogonal to the target, and where the growth rate is correspondingly small), on centring the plume on the edge of the sample [19], on scanning the substrate in two orthogonal directions [20], or on rastering the laser beam across a large target [21].

In our apparatus, the substrate translation and laser firing are easily synchronized. Therefore, for a substrate that is simultaneously rotated about its centre, and translated through the centre of the plume in an oscillatory fashion, the laser firing can be chosen such that more pulses are fired near the edge of the substrate than at its centre.

However, determining the correct combination of laser firing and substrate motion is complicated by the fact that the size of a typical 2 inch substrate is comparable to that of the full-width at half-maximum (FWHM) of the deposition profile associated with a single laser pulse. In contrast, if the substrate were much larger, it would obviously be appropriate to fire the laser pulses at positions such that the number of pulses fired at a radial position  $r$  is given by  $\rho(r) \propto r$ . Note that this type of profile would be impossible if the laser repetition were kept constant and the substrate were translated with a variable velocity, as an infinite speed at the origin would be required. However, defining ‘trigger points’, i.e., physical substrate translation positions at which the laser is fired, is sufficient to obtain this dependence.

Not surprisingly, in our test experiments of the deposition of  $\text{CeO}_2$  in a background pressure  $p \leq 10^{-5}$  Torr, this type of profile was not appropriate and resulted in a minimum thickness at the centre of the substrate. This is an obvious consequence of the finite width of the deposition profile

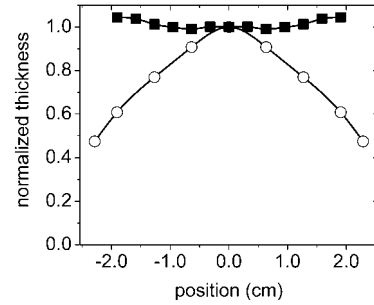


**Figure 2.** Film thickness as a function of radial position on a circular sample, for the case of  $\text{CeO}_2$  deposited in vacuum, without the use of an aperture between the target and the substrate. Open circles represent the profile obtained by simple substrate rotation, full squares that by a combination of translation and rotation, and a position-dependent laser firing as described in the text.

associated with each laser pulse. However, the profile can easily be generalized as

$$\rho(r) \propto r^\alpha + \beta. \quad (1)$$

In figure 2, the profile resulting from  $\alpha = 1$  and  $\beta = 0.1$  is compared to that resulting from the growth without translation of the substrate. Clearly, the obtained uniformity ( $\pm 5\%$  across the entire area) is sufficient for many applications.

### Uniform-thickness growth on a line of samples

Many applications, including the temperature-gradient growth optimization described below, necessitate the deposition of a thin film on a series of samples that are placed in a linear arrangement on a substrate holder. To achieve this type of deposition, the sample holder is translated laterally during deposition in an oscillatory fashion. Wear and tear in mechanical actuators often relate to the acceleration rather than the maximum velocity of moving parts. Therefore, we minimize the acceleration by choosing a time dependence as shown in figure 3(a), resulting in a ‘saw-tooth’ velocity (time) profile. The corresponding position (time) curve is shown in figure 3(b).

If we define  $T$  as the time required to travel between the extremes of the oscillation, then the maximum velocity  $v_m$  is given by

$$\frac{T}{2} = \frac{v_m}{a}, \quad (2)$$

where  $a$  is the acceleration. Therefore, the maximum position is

$$p(T/2) = \frac{v_m^2}{2a}. \quad (3)$$

If we impose the maximum position and the oscillation time, the required acceleration is immediately found as

$$a = \frac{2v_m}{T} = \frac{2p(T/2)}{T^2}. \quad (4)$$

During the deposition, the laser can be fired either by position-dependent trigger signals, or at a constant repetition rate. For a constant repetition rate, the substrate travels a variable distance between two laser shots due to the variable velocity. Therefore, it is illustrative to consider the velocity as a function

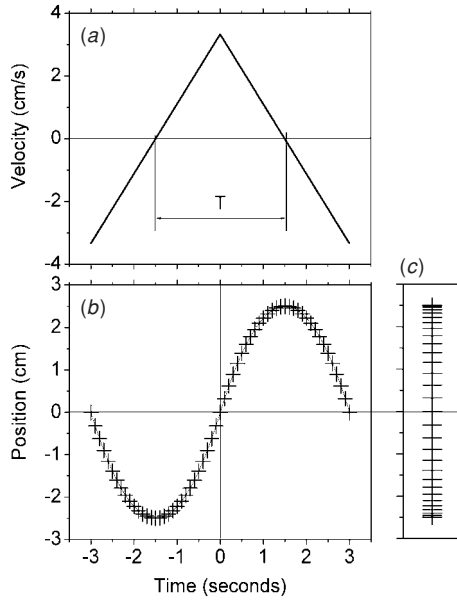


**Figure 3.** Substrate plate velocity and position as a function of time, for the actual parameters used in our experiments. Plus signs in (b) indicate the location of the substrate at the time of each laser firing. These locations are shown in (c) as a function of position.

of position,

$$v(p) = \sqrt{v_m^2 - 2ap}. \quad (5)$$

The distance travelled between two laser shots is proportional to the inverse of  $v(p)$ , and therefore reaches its maximum value at  $p = 0$  and approaches zero for the extreme positions.

In figure 3(b), the position (time) profile is drawn for the actual conditions used in our experiments. If the laser is fired at a repetition rate of 10 Hz, the crosses shown in the figure correspond to the location of the substrate at the time of each laser firing. In figure 3(c), these locations are shown as a function of position, illustrating clearly the dense spacing near the end points of the travel range.

To calculate the expected deposition profile, we make the simple assumption for the spatial distribution of the material deposited by each laser pulse centred at  $x_i$  to be a Gaussian profile with a full-width at half-maximum (FWHM) of  $w$ :

$$d_i(x) = r \exp \left\{ -4 \ln 2 \left( \frac{x - x_i}{w} \right)^2 \right\}. \quad (6)$$

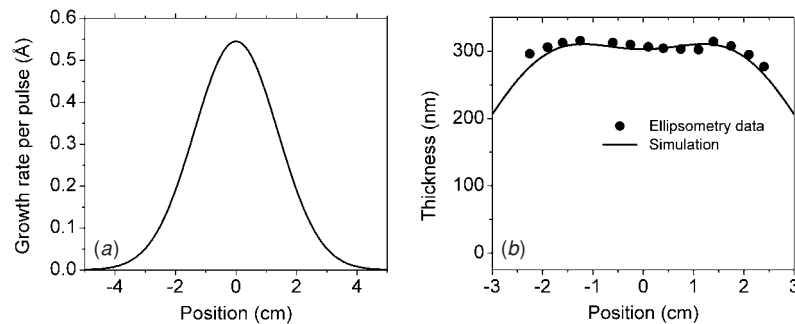


**Figure 4.** (a) Deposition profile for a single laser pulse, calculated as a Gaussian curve (equation (6)) with a FWHM  $w = 3.25$  cm. (b) Superposition of curves as shown in (a) for all positions given in figure 3(c), as compared to the data from our [21].

Here,  $r$  is a deposition rate per pulse. In figure 4(a), this profile is drawn for  $r = 0.545$  Å/pulse and  $w = 3.25$  cm.

Superposition of Gaussian curves as given in equation (6) for each location as shown in figure 3(c) then gives the total thickness distribution across the heater plate:

$$d(x) = N \sum_i d_i(x) \quad (7)$$

where  $N$  is the number of passes made by the substrate during the entire deposition.

Figure 4(b) shows the curve obtained by equation (7) together with our data (from [21]). Clearly, the agreement is very satisfactory.

These experiments show that a simple oscillatory motion, coupled with a constant laser repetition rate, yields a sufficiently uniform thickness-profile across a heater plate. The region of uniformity is comparable to the total travel distance of the oscillatory substrate motion. Simple assumptions (such as a Gaussian deposition rate profile for an individual laser pulse) are sufficient to understand how this uniformity is obtained. Clearly, by increasing the laser repetition rate near the centre and near the edges, the uniformity could be further optimized.

### A parallel approach to growth-temperature optimization

As a prerequisite for any study on thin films of complex materials, single-phase layers with excellent crystalline quality must be obtained. The optimization of the relevant growth parameters, in particular the deposition temperature, is time consuming, and several research groups have implemented ‘multi-sample’ approaches. However, the use of a variable-temperature substrate heater has only recently been applied to complex oxides [23, 24].

In this section, we describe the technical implementation and performance specifics of a temperature-gradient method based on conventional radiative heating of a metallic substrate holder, using an exposed Pt-based filament. The apparatus is based on—and integrated with—the approach to obtain a uniform coating on a row of samples as presented in the previous section. After describing the technical details, we show the application of this method to the ferroelectric complex oxide, strontium barium niobate ( $\text{Sr}_x\text{Ba}_{1-x}\text{Nb}_2\text{O}_6$ : SBN).

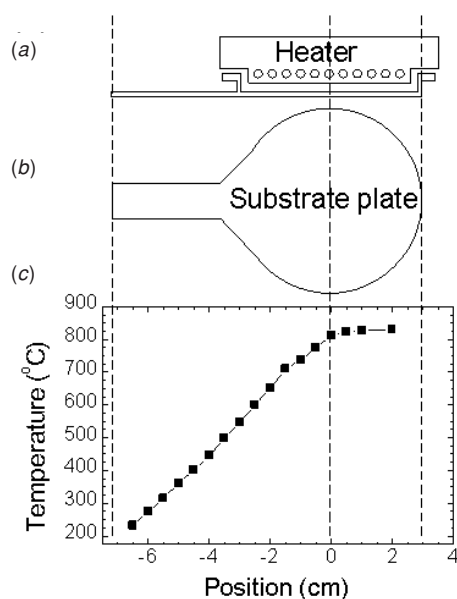


**Figure 5.** (a) Side view and (b) front view schematic of the temperature-gradient substrate holder, and (c) the temperature variation as a function of the position.

#### Technical approach

In our implementation, the temperature gradient over the film deposition surface is achieved by placing a specially designed substrate plate, as shown in figures 5(a) and (b), in front of a 6.3 cm diameter radiative heater (capable of operation above 800 °C in air).

Here, an intentionally asymmetric radiation loss combined with the limited thermal conduction within the metallic plate leads to a reproducible gradient covering a range of temperatures from 200 °C to 830 °C over a distance of 7.5 cm and in an oxygen background pressure between 100 mTorr and  $1 \times 10^{-6}$  Torr. In initial test runs, the temperature at 18 points on the substrate holder was measured by individual thermocouples and shown to be highly reproducible (in fact, the 18 data points in figure 5(c) were obtained on six separate runs). A two-colour pyrometer is then used for minor run-to-run adjustments of the heater power. During film growth onto this temperature-gradient substrate holder, thickness variations of less than 15% across the area of interest for this study (500–830 °C) are achieved by the oscillatory substrate motion as described above.

#### Application to electro-optic materials (SBN)

SBN is an attractive ferroelectric material because it exhibits an exceptionally large electro-optic (EO) coefficient,  $r_{33}$ , making it a potential material of choice for miniaturized EO modulators, real-time holography applications and information storage technologies. In particular,  $r_{33}$  can be varied by changing compositions ratio of Sr and Ba, thus achieving values of  $r_{33}$  10–40 times larger than obtained on congruently grown lithium niobate, the current industry standard [25].

$\text{Sr}_{0.5}\text{Ba}_{0.5}\text{Nb}_2\text{O}_6$  (SBN:50) films were deposited at an oxygen pressure of 15 mTorr, utilizing a laser repetition rate

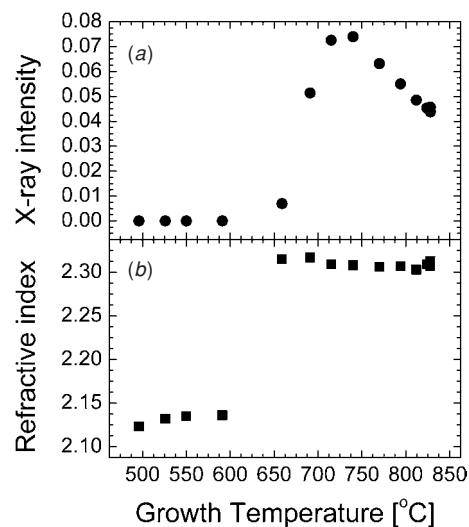


**Figure 6.** (a) X-ray intensity of the (002)-reflection (normalized with respect to film thickness and substrate peak intensity) measured on SBN films obtained using the temperature-gradient approach. (b) Refractive index at 2.0 eV of the same samples.

of 10 Hz and an energy density of  $3.8 \text{ J cm}^{-2}$ , and using ceramic SBN:50 targets placed at a distance of 6.5 cm from the MgO(001) substrates.

X-ray diffraction results obtained on a series of simultaneously deposited SBN films show that crystallization occurs with an SBN[001]/MgO[001] epitaxial relationship (see [25]). To visualize the evolution of the crystallinity as a function of growth temperature, we normalize the intensity of the SBN(002) reflection peak  $I_{\text{SBN}(002)}$  with respect to the intensity corresponding to the MgO(002) reflection ( $I_{\text{MgO}(002)}$ ) and the slightly varying film thickness  $d$ , i.e.  $I_{\text{norm}} = I_{\text{SBN}(002)} / (I_{\text{MgO}(002)} d)$ .

As shown in figure 6(a), strong crystallization occurs at temperatures above 650–700 °C, with the strongest values of  $I_{\text{norm}}$  observed between 700 °C and 750 °C. At higher substrate temperatures, the x-ray intensity corresponding to this normal orientation decreases. In figure 6(b), we show the refractive index at 2.0 eV as determined by ellipsometry [22]. An almost step-like change is observed between 600 °C and 650 °C, with no further change at higher temperatures. Since optical properties are a measure of the local coordination in the material, this dependence indicates that crystallization starts to occur around 600 °C but full grain growth requires temperatures of at least 700 °C. The decrease in x-ray intensity above 750 °C (in a regime where the optical properties and thus the short-range structure do not change) is therefore interpreted in terms of a poorer epitaxial relationship between the substrate and the film, and a broader distribution of grain orientations.

To summarize, a temperature-gradient apparatus based on radiative substrate heating allows us to simultaneously deposit thin films onto multiple samples at different growth temperatures spanning a range of 500 °C. For a series of  $\text{Sr}_{0.5}\text{Ba}_{0.5}\text{Nb}_2\text{O}_6$  films on MgO(001) substrates, variations in optical and structural properties were clearly observed as a function of growth temperature.

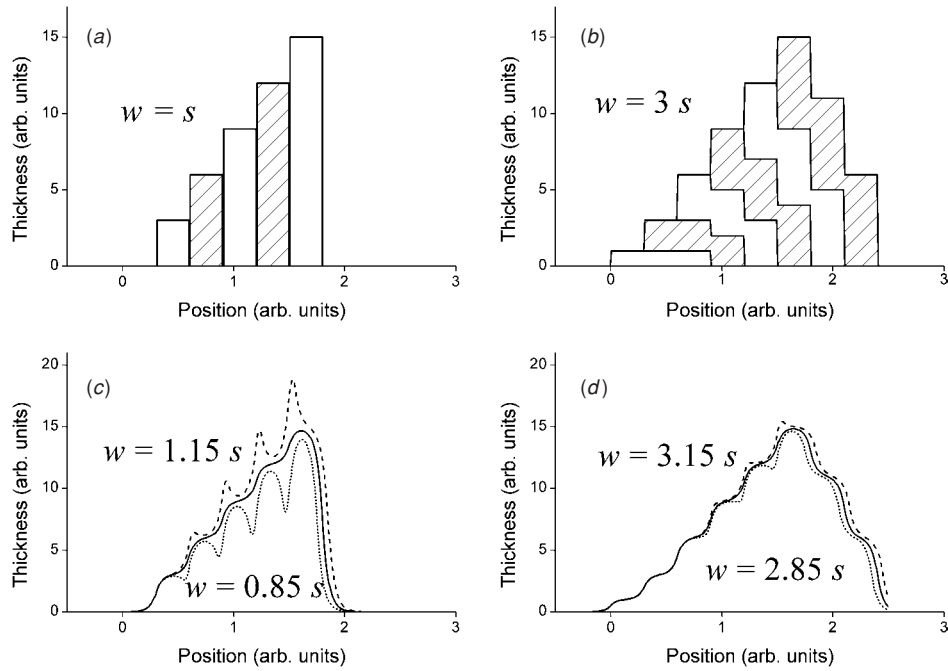


**Figure 7.** Illustration of the approach (a) in which the width of the line-shaped profile deposited on the substrate is equal to the step size ( $w = s$ ) and (b) in which  $w = 3s$ ; for ideally sharp lines. Broadening of the deposited lines yields the profiles indicated by solid lines in (c) and (d). Also shown as dashed and dotted lines in (c) and (d) are profiles calculated for erroneous values of  $w$ .

### A parallel approach based on spatial variations of film thickness

#### *Controlled deposition of wedge-shaped thickness profiles*

As discussed in the introduction, CCS fundamentally relies on an intentional spatial variation of the deposition rate, equivalent to the deposition of wedge-shaped thickness profiles of thin films. Two wedges having opposite or orthogonal orientations and corresponding to different composition can either be deposited simultaneously [1, 4, 6, 26, 27] or sequentially [7, 9, 11, 14, 15, 28].

For the reasons discussed above, obtaining well-controlled profiles over large substrate areas ( $\geq 2-3$  cm) requires an approach in which the substrate is translated behind an aperture rather than a moving-shield technique. Obtaining such profiles is rather straightforward; however, it is significantly more complicated than in a moving-mask technique (where a simple constant-velocity translation of that shield in combination with a constant deposition rate suffices). Here, either the translation velocity or the deposition rate must continuously vary during each pass.

Pulsed-laser deposition is particularly suited for this approach because the deposition is ‘quantized’ and can be precisely controlled using simple automation techniques. With an aperture in the shape of a slit, each laser pulse will deposit a rectangular-shaped ‘line’ across the substrate, having a width  $w$ . The sample is then moved in finite steps by a distance  $s$ . Note that the use of simple laser-beam scanning in the direction parallel to this slit-shaped aperture yields good average uniformity along the profile.

In figure 7, we show two basic possibilities: (a) illustrates the case where the substrate is moved in steps that are equal

in size to the width of the deposition profile (i.e.,  $w = s$ ), and at each point, an incrementally larger amount is deposited; (b) illustrates the case where the slit is wide compared to the step size ( $w = 3s$ ). These curves are obtained under the assumption of an ideally sharp profile. However, due to the physical distance between the shield and the substrate, the deposition lines will be broadened. In figures 7(c) and (d), the solid lines are the profiles corresponding to those in (a) and (b), re-calculated with the assumption of a broadening (‘smearing-out’) of the lines by an amount  $0.15s$ .

The most significant difference between the two approaches is the slight nonlinearity for the case of  $w > s$ . In fact, it is readily seen that the profile is nonlinear for the first distance  $L_{NL}$ , given by the overlap between successive deposition lines:

$$L_{NL} = w - s. \quad (8)$$

In addition to broadening of lines, in real experiments the actual line width may be slightly different from the ideal value. An error of  $0.15s$  was assumed for some of the calculations in figures 7(c) and (d). The dotted lines correspond to an underestimate, the dashed lines to an overestimate.

Here, distinct differences between the two approaches are observed: clearly, a method where the line width is large compared to the step size is much more ‘robust’ than the case of  $s = w$ .

The effect of line broadening and asymmetry is illustrated by the calculations presented in figure 8. Cases (a) and (b) correspond to the ideal and slightly broadened examples of figure 7. Despite the small nonlinearity near the beginning and the end of the wedge, the overall quality of the profile is excellent. Further broadening (case (c)) yields an even smoother variation of the thickness; however, there is an

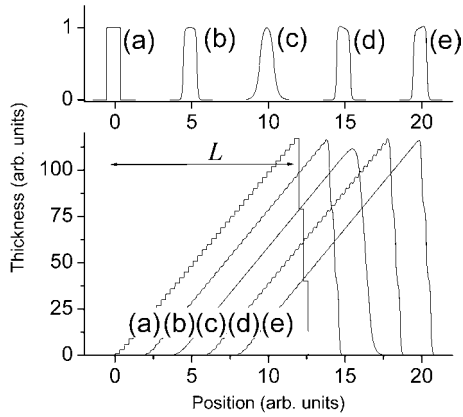


**Figure 8.** Effect of line shape on the resulting ‘wedges’. Cases (a), (b) and (c) are symmetric profiles with varying degrees of broadening, and (d) and (e) are broadened to the same extent as (b), but are asymmetric. In all cases, the overall linearity of the wedge is preserved.

additional deviation from the desired profile near its beginning and its end.

Finally, cases (d) and (e) illustrate the situation for asymmetric lines. Such lines can occur when the plume and the aperture are strongly misaligned. As these calculations indicate, even in this case, the overall linearity of the profile is preserved. This shows the inherent robustness of this approach.

#### Practical considerations

In a typical experimental configuration, the width of the line ( $w$ ), the growth rate per pulse ( $d$ ), the thickness  $D$  at the thickest point and the distance  $L$  (see figure 8) over which the entire wedge should be deposited are the imposed parameters. The step size ( $s$ ) and the number of steps ( $N$ ) are then to be determined. The pulsed nature of the process obviously limits the use of  $s$  to values for which  $w = ks$ , where  $k$  is an integer, and therefore not all combinations of  $w$ ,  $d$ ,  $D$  and  $L$  are possible.

Therefore, for a typical experiment, it is useful to first determine an initial (‘desired’) value  $D_d$ , for which the parameters  $s$  and  $N$  are then determined. Because some combinations of  $s$  and  $N$  are incompatible with the experimental  $w$ , the value of  $s$  must be adjusted. The actual value of  $D_a$  is then re-calculated. For  $N \gg w/s$ , we will find that  $D_a \approx D_d$ .

For these calculations, we first note that for values of  $N$  such that  $N \gg w/s$ , the total thickness can be approximated as

$$D_d \approx dNw/s. \quad (9)$$

Obviously, the total length of the profile is given by

$$L = Ns. \quad (10)$$

Combining equations (9) and (10), one finds

$$s \approx \sqrt{\frac{d}{D_d}}Lw. \quad (11)$$

Using the result of equation (11), the ratio  $w/s$  will in general not be an integer. For sufficiently small growth rates  $d$

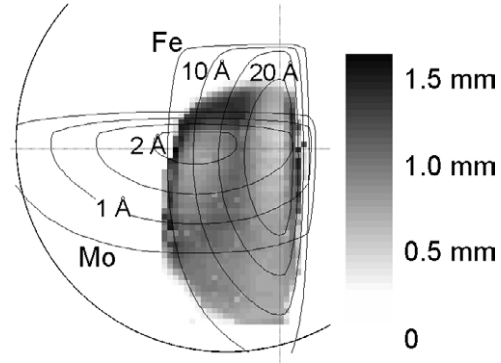


**Figure 9.** Application of metallic wedges to the study of catalysis for nanotube synthesis. The contours show the thickness of the two metallic films deposited by PLD (Mo followed by Fe). The grey scale indicates the length of the carbon nanotubes in the dense forest grown by CVD (measured by optical profilometry).

per pulse,  $w/s$  will be quite large (typical values in our experimental configuration range from 10 to 100), and can easily be rounded to the nearest integer.

With the value of  $s$  now determined,  $N$  is calculated from equation (10), and the correct value of  $D_a$  is obtained from

$$D_a = d \frac{w}{s} \left( N - \frac{w-s}{2s} \right). \quad (12)$$

Once again, it is readily seen that for  $N \gg w/s$ , equation (12) reduces to equation (9).

Finally, it is worthwhile to note that for a sufficiently broadened profile, the requirement of  $w = ks$ , where  $k$  is an integer, can be lifted, and the determination of the parameters becomes trivial.

#### Optimization of catalysts for long-length carbon nanotube growth

Carbon nanotubes (CNTs) are readily grown by a catalytic process using either an ethylene- [29], methane- [30] or acetylene-based [31] CVD method. Bi-metallic catalysts appear to exhibit synergistic advantages in producing CNTs from hydrocarbons [32, 33], and Fe–Mo alloys in particular have been used for the growth of single-walled [32, 34–36] and multiwalled [37] nanotubes.

Despite the significance of optimizing catalyst composition, there have been relatively few studies that systematically investigate the dependence of CNT characteristics on the catalyst composition, due to the time-consuming nature of such studies. The approach described here to obtain thin layers of metals is ideally suited for such a study.

In fact, our method allows us to study simultaneously the effect of catalyst composition and quantity of a binary metallic alloy.

Substrates were prepared by e-beam evaporation of 100 Å of Al onto Si wafers, which were then transferred to the PLD system for the fabrication of the catalysts. The sequential deposition of a Mo wedge (bottom) and a Fe wedge (top), rotated with respect to each other by 90°, thus yields two overlapping profiles as shown in figure 9, such that each point

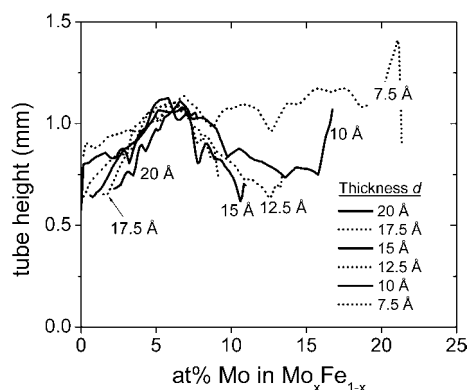


**Figure 10.** Carbon nanotube height as a function of catalyst composition for various amounts of catalyst (thickness  $d$ ). Data re-plotted from figure 9. A clear maximum at  $x \approx 0.6$  is observed independently of  $d$ .

on the substrate is covered first by a layer of Mo (with a thickness  $d(\text{Mo})$ ) and a top layer of Fe (with a thickness  $d(\text{Fe})$ ). Different positions on the substrate therefore correspond to different  $d(\text{Mo})/d(\text{Fe})$  ratios and different  $d(\text{Mo}) + d(\text{Fe})$  amounts. The sample is then transferred to a tube furnace and heated to 730 °C in flowing  $\text{H}_2/\text{Ar}$  gas, followed by a 1 h exposure to flowing acetylene ( $\text{C}_2\text{H}_2$ ). More details can be found in [38].

During this CVD process, a dense forest of vertically aligned nanotubes grows on the portion of the substrate containing the Fe catalyst; within this region, however, the height of the tubes depends strongly on position, as illustrated by the two-dimensional map of the forest's height (figure 9).

TEM analysis (see [38]) shows that the catalyst nanoparticles formed in this process are alloys of  $\text{Mo}_x\text{Fe}_{1-x}$ , with a composition corresponding to the individual amounts of Mo and Fe deposited at each location.

In order to better understand the dependence of tube length on catalyst composition, the data can be shown as a function of the average catalyst composition  $x$  in  $\text{Mo}_x\text{Fe}_{1-x}$  and of the catalyst amount  $d = d(\text{Mo}) + d(\text{Fe})$ . As is clearly observed in figure 10, a strong local maximum in tube height occurs for a composition  $x \approx 0.06$ , and independent of catalyst thickness  $d$  in the range  $5 \text{ \AA} \leq d \leq 20 \text{ \AA}$ .

This observation of a composition-dependent maximization of CNT height is clearly of significant technological importance. In fact, while in our earlier growth runs the quantities  $d(\text{Mo})$  and  $d(\text{Fe})$  had to be carefully adjusted, our results indicate that tall forests can be grown by CVD by controlling only the average composition  $x$  of the  $\text{Mo}_x\text{Fe}_{1-x}$  catalyst. This can very easily be achieved, for example in solution-deposition approaches, or by sputtering or laser ablating from a target of that composition.

The scientific impact of this observation is similarly important. In fact, catalysis of carbon nanostructures is still poorly understood, and the clearly visualized trends in our sets of data provide a reliable test-bed for models of catalytic processes.

The results thus clearly illustrate the utility of a CCS method based on thin wedge profiles.

### ***In situ* alloy formation in continuous compositional spread**

As described in the introduction, an alloy (or solid solution)—even a metastable phase—can be obtained by a method of repeated sequential deposition of monolayer amounts of each of the constituents. If each material is deposited in a way that would by itself lead to a wedge-shaped thickness profile, and the different constituents are deposited with profiles that have different spatial orientations, a composition-spread sample is obtained.

In our experiments, we found that the method described above for the deposition of thin wedges is inappropriate for this application. This wedge-deposition method has proved to be appropriate for the deposition of very thin layers (maximum thickness in the order of 10 Å–100 Å), with a well-defined zero-thickness end point, such as was needed for the study of catalysis (see above).

Compositional spread is typically used for much thicker layers, but in each step in the sequential deposition (such as to allow for *in situ* mixing and the formation of metastable compounds), an amount of less than a unit cell of the material must be deposited before cycling to the other constituent.

Therefore, the apparently similar situations (wedge deposition and continuous compositional spread) are best treated with significantly different approaches.

#### *Basic approach*

For the deposition of composition spreads, the substrate is again passed behind the slit-shaped aperture and the laser is fired at pre-defined ‘trigger points’. Here, instead of using equally spaced points at which a gradually increasing number of laser pulses are fired (as described above), the trigger points are non-equally spaced such that firing one laser shot per trigger point now leads to the desired spatial variation of the composition. The obvious advantage of this approach is that the substrate motion can be continuous and rapid, hence drastically reducing the time required for the approach based on hundreds of passes.

After one pass, during which less than one monolayer of the material must be deposited, the target is exchanged, a different set of trigger points for the second material is chosen, and the substrate is passed behind the aperture again. Figure 11 illustrates this procedure schematically.

In order to obtain a composition that varies linearly from left to right across the substrate, both constituents have to be deposited with linear spatial deposition-rate profiles. In other words, the deposition of each constituent must be such that if deposited by itself, the resulting film would again have a ‘wedge’-type thickness profile ( $t(x) = t_0 + ax$ ).

As before, each laser pulse leads to the deposition of a finite and equal amount of material in the narrow region of the aperture slit. With an appropriate slit-to-substrate distance, this deposition can be described as a smudged line perpendicular to the direction of the composition gradient, with a cross-section that roughly follows a Gaussian shape. We therefore need to approximate the linear profile as a superposition of  $N$  Gaussians centred at  $x_i$  (these values are then used as ‘trigger points’ during the deposition).

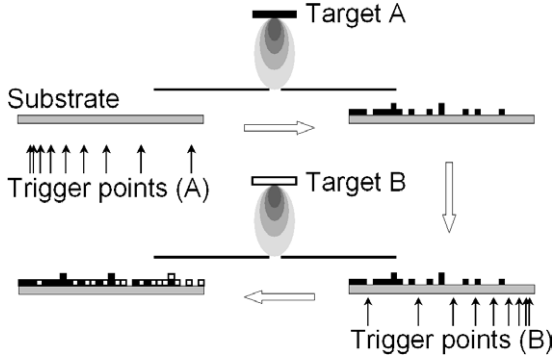


**Figure 11.** Compositional-spread method allowing for *in situ* alloying and thus the formation of metastable phases. The substrate repeatedly passes behind a slit-shaped aperture, and the laser is fired whenever the substrate position coincides with one of the predetermined ‘trigger points’. Less than one monolayer of the material is deposited in each cycle.

Simple geometrical arguments show that a linear profile  $t(x) = t_0 + ax$  can be approximated by such a superposition if successive trigger points are spaced by

$$\delta x_i = -\sum_{n=1}^{i-1} \delta x_n - \frac{t_0}{a} + \sqrt{\left[\sum_{n=1}^{i-1} \delta x_n + \frac{t_0}{a}\right]^2 + 2\delta x_1 \frac{t_0}{a} + \delta x_1^2}. \quad (13)$$

$\delta x_1$  is chosen iteratively such that the desired length of the profile corresponds to

$$L = x_N + \frac{\delta x_N}{2}. \quad (14)$$

A small number of trigger points can obviously not lead to a smooth profile. In fact, for our typical geometry (3 mm wide slit, and a compositional spread across a 3 cm range), more than 100 trigger points are necessary (see [28] for more details). This could, in principle, lead to more than one monolayer of material being deposited per pass. In order to avoid this situation, the complete set of trigger points  $x_n$  is first calculated, but only a subset is used for each pass: for example, in pass one, the laser can be fired for  $n = 0, 5, 10$ , etc, in pass two for  $n = 1, 6, 11$ , etc.

As in all CCS approaches, the composition  $c(x)$  at each point  $x$  varies uniformly along the direction of the spread. Therefore, any sample of finite size  $\Delta x$  bears a compositional variation of  $\Delta c = (\delta c / \delta x) \Delta x$ . The composition slope  $(\delta c / \delta x)$  depends both on the range of compositions investigated ( $\Delta c^{\max}$ ) and the linear size of the spread ( $\Delta x^{\max}$ ), so that the composition non-uniformity of each sample is given by

$$\Delta c = \frac{\Delta c^{\max}}{\Delta x^{\max}} \Delta x. \quad (15)$$

For example, in the case of an alloy  $A_x B_{1-x}$ ,  $\Delta c^{\max} = 1$  if the entire range  $0 \leq x \leq 1$  is investigated, but  $\Delta c^{\max} = 0.1$  if only alloys between  $A_{0.3} B_{0.7}$  and  $A_{0.4} B_{0.6}$  are of interest. For the examples of  $(Sr_{1-x} Ca_x) RuO_3$  composition spreads given below,  $\Delta c^{\max} = 1$  and  $\Delta x^{\max} = 27$  mm, thus for a 2 mm wide sample,  $\Delta c = 7.5\%$ . This is sufficient for initial studies and the observation of general trends but can complicate detailed investigations. Therefore, such studies require a narrower

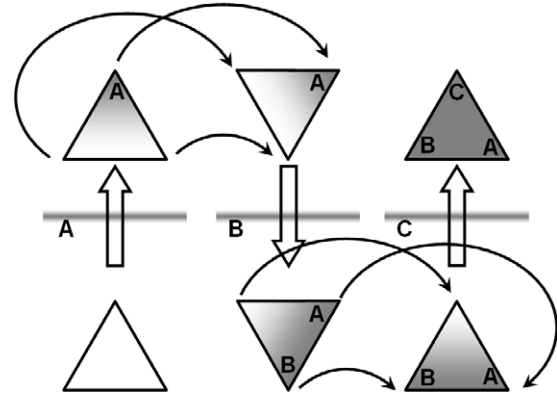


**Figure 12.** Basic principle for the formation of ternary phase diagrams. Trigger points are set similarly to the case shown in figure 11; however, the substrate is rotated by  $60^\circ$  between each pass behind the slit-shaped aperture.

concentration range (e.g.,  $\Delta c^{\max} = 0.1$ ) chosen in the area of interest. Using our apparatus’ capability of  $\Delta x^{\max} \geq 40$  mm, a value of  $\Delta c \leq 0.005$  can then readily be obtained.

Finally, it is possible to use the apparatus as described to grow (by simple two-target mixing and keeping the substrate stationary) uniform-composition films of any of the materials within a compositional spread, allowing for direct confirmation of the results and further detailed examination of samples with specific compositions.

#### Generalization to two-dimensional (two-parameter) problems

The above section describes a CCS approach for a binary system, with the composition varying linearly along one spatial direction of the substrate. This application is simple because it does not require good deposition-rate uniformity in the direction parallel to the slit-shaped aperture. Fortunately, simple laser-beam scanning along this slit can result in uniformity along that direction on length scales comparable to those utilized for the substrate translation, and thus the approach can easily be adapted to two-dimensional problems.

The simplest generalization of the approach is the case in which the two ‘wedge-type’ profiles are deposited not as mirror images of each other, but rotated by  $90^\circ$ , then the resulting spatial variation across the substrate will allow for the simultaneous study of composition and film thickness, similar to the method described above, but now applicable to *in situ* mixing and thus for the formation of metastable phases.

Similarly, it is easy to generalize the approach to ternary systems: as illustrated in figure 12, a rotation of the substrate by  $60^\circ$  between the deposition steps of the individual constituents suffices to obtain all compositions of an entire ternary phase diagram.

#### Example: $(Sr_{1-x} Ca_x) RuO_3$ composition spreads

Binary composition-spread films of  $(Sr_{1-x} Ca_x) RuO_3$  were grown according to the procedure described above, with a total film thickness of about 250 nm. Commercially available  $SrRuO_3$  and  $CaRuO_3$  targets were used for this study. Eight individual substrates of  $LaAlO_3$  (each measuring  $5 \times 10$  mm<sup>2</sup>)

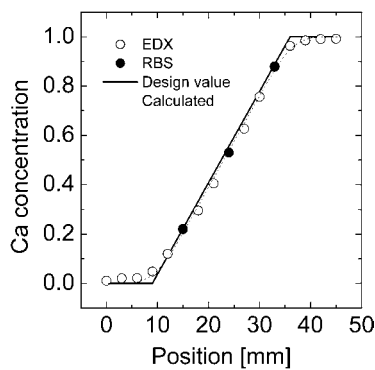


**Figure 13.** Compositional analysis of  $\text{Sr}_{1-x}\text{Ca}_x\text{RuO}_3$  samples obtained in a single deposition run. Open and full circles represent data from EDX and RBS, respectively. The solid line indicates the profile as attempted, whereas the broken line shows the results from calculations taking into account the broadening of the deposition area and a small lateral offset between laser spot and aperture centre.

were mounted on the heater plate at  $675\text{ }^\circ\text{C}$  within an area of  $45 \times 10\text{ mm}^2$  (i.e., leaving less than 1 mm space between adjacent pieces). For detailed characterization, these samples were cut into  $2 \times 10\text{ mm}^2$  slabs after deposition. Figure 13 shows measurements of the composition  $c^{\text{meas}}(x)$  as a function of position  $x$  on the heater plate. The solid line indicates the profile  $c^{\text{design}}(x)$  as entered into the control software. Measurements were performed using energy dispersive x-ray spectroscopy (EDX) in a scanning electron microscope, and by Rutherford backscattering spectroscopy (RBS); these two methods show agreement well within the expected experimental errors.

As is clearly seen, the experimental data agree well with the desired values for the composition. Two types of systematic deviations are nevertheless observed: first, there is clearly some ‘rounding’ in the profile near the inflection points at 9 mm and 36 mm. This is expected for an aperture consisting of a slit with finite width. Furthermore, the experimental data points are systematically shifted by about 1 mm due to imperfect alignment of the system (laser spot, centre of the aperture and ‘zero position’ on the heater position not falling onto a perfectly straight line). Taking these two effects into consideration, the expected composition variation  $c^{\text{calc}}(x)$  can be calculated (by a superposition of Gaussian profiles centred at the ‘trigger points’) and is shown as a broken line in figure 13.

The  $(\text{Sr}_{1-x}\text{Ca}_x)\text{RuO}_3$  films on  $\text{LaAlO}_3$  substrates (cut into pieces measuring  $2 \times 10\text{ mm}^2$ ) have been characterized using standard x-ray diffraction to determine their out-of-plane lattice parameters, and the sample’s electrical resistance was measured as a function of temperature.

These results [28] (not shown here) demonstrate that the films obtained by this method are comparable (quantitatively and qualitatively) to individual samples grown by our group and others.

## Conclusions

We have introduced a generalized, PLD-based CCS approach, and have shown that this method can be used to obtain controlled lateral variations of film thickness, film

composition, or deposition temperature. In all cases, the resulting samples are sufficiently large for conventional characterization and measurement techniques, including ellipsometry, SQUID magnetometry, resistance-versus-temperature measurements, etc.

Our technique is based on a flexible PLD apparatus with precise, rapid synchronization between substrate rotation and translation, target exchange and laser firing. The use of a fixed, slit-shaped aperture between the moving substrate and the target results in uniform deposition kinetics and growth rates (by selecting only the central portion of the plume for all positions on the substrate), and enables controlled linear variations on sufficient sample size.

In this paper, we have presented the basic technical details and control algorithms, and described some key results from our experiments on electro-optic materials, ferromagnetic oxides and catalysts for carbon nanotube synthesis. These results indicate the wide range of applications of such a conceptually simple technique. Integration of this method into a more comprehensive study of the physical systems under investigation yields a significant increase in the speed of discovery and optimization.

## Acknowledgments

Research sponsored by the US Department of Energy under contract DE-AC05-00OR22725 with the Oak Ridge National Laboratory, managed by UT-Battelle, LLC.

## References

- [1] Kennedy K 1965 *Atomic Energy Commission Report* UCRL-16393
- [2] Sawatzky E and Kay E 1969 Cation deficiencies in r.f. sputtered gadolinium iron garnet films *IBM J. Res. Dev.* **13** 696–702
- [3] Gavaler J R, Janocko M A and Jones C K 1974 Preparation and properties of high- $T_c$  Nb–Ge films *J. Appl. Phys.* **45** 3009–13
- [4] van Dover R B, Schneemeyer L F and Fleming R M 1998 Discovery of a useful thin-film dielectric using a composition-spread approach *Nature* **392** 162–4
- [5] Wang Q *et al* 2002 Combinatorial synthesis of solid state electronic materials for renewable energy applications *Appl. Surf. Sci.* **189** 271–6
- [6] Perkins J D *et al* 2002 Combinatorial studies of Zn–Al–O and Zn–Sn–O transparent conducting oxide thin films *Thin Solid Films* **411** 152–60
- [7] Christen H M, Silliman S D and Harshavardhan K S 2001 Continuous compositional-spread technique based on pulsed-laser deposition and applied to the growth of epitaxial films *Rev. Sci. Instrum.* **72** 2673–8
- [8] Christen H M, Silliman S D and Harshavardhana K S 2002 Epitaxial superlattices grown by a PLD-based continuous compositional-spread technique *Appl. Surf. Sci.* **189** 216–21
- [9] Yoo Y-K *et al* 2000 Room-temperature electronic phase transitions in the continuous phase diagrams of perovskite manganites *Nature* **406** 704–8
- [10] Li J *et al* 2000 Electro-optic measurements of the ferroelectric–paraelectric boundary in  $\text{Ba}_{1-x}\text{Sr}_x\text{TiO}_3$  materials chips *Appl. Phys. Lett.* **76** 769
- [11] Danielson E *et al* 1997 A combinatorial approach to the discovery and optimization of luminescent materials *Nature* **389** 944–8

- [12] Christen H M *et al* 1998 Pulsed laser deposition of solid-solution films using segmented targets *Thin Solid Films* **312** 156–9
- [13] Mieville L *et al* 1997 Ti and Ca substitution in SrRuO<sub>3</sub> thin films by sequential deposition process *Appl. Phys. Lett.* **70** 126–8
- [14] Fukumura T *et al* 2000 Rapid construction of a phase diagram of doped Mott insulators with a composition-spread approach *Appl. Phys. Lett.* **77** 3426–8
- [15] Chang K S *et al* 2001 Multimode quantitative scanning microwave microscopy of *in situ* grown epitaxial Ba<sub>1-x</sub>Sr<sub>x</sub>TiO<sub>3</sub> composition spreads *Appl. Phys. Lett.* **79** 4411–3
- [16] Chang H, Takeuchi I and Xiang X-D 1999 A low-loss composition region identified from a thin-film composition spread of (Ba<sub>1-x-y</sub>Sr<sub>x</sub>Ca<sub>y</sub>)TiO<sub>3</sub> *Appl. Phys. Lett.* **74** 1165–7
- [17] Chrisey D B and Hubler G K (ed) 1994 *Pulsed Laser Deposition of Thin Films* (New York: Wiley)
- [18] Lowndes D H *et al* 1996 Synthesis of novel thin-film materials by pulsed laser deposition *Science* **273** 898–903
- [19] Foltyn S R *et al* 1991 Large-area two-sided superconducting YBa<sub>2</sub>Cu<sub>3</sub>O<sub>7-x</sub> films deposited by pulsed laser deposition *Appl. Phys. Lett.* **59** 1374–6
- [20] Davis M F *et al* 1991 Deposition of high quality YBa<sub>2</sub>Cu<sub>3</sub>O<sub>7-δ</sub> thin films over large areas by pulsed laser ablation with substrate scanning *J. Appl. Phys.* **69** 7182–8
- [21] Greer J A 1992 High quality YBCO films grown over large areas by pulsed laser deposition *J. Vac. Sci. Technol. A (Vac. Surf. Films)* **10** 1821–6
- [22] Ohkubo I *et al* 2004 High-throughput growth temperature optimization of ferroelectric Sr<sub>1-x</sub>Ba<sub>x</sub>Nb<sub>2</sub>O<sub>6</sub> epitaxial thin films using a temperature gradient method *Appl. Phys. Lett.* **84** 1350–2
- [23] Koida T *et al* 2002 Temperature-gradient epitaxy under *in situ* growth mode diagnostics by scanning reflection high-energy electron diffraction *Appl. Phys. Lett.* **80** 565–7
- [24] Nishimura J *et al* 2003 Fabrication of spin-frustrated Sm<sub>2</sub>Mo<sub>2</sub>O<sub>7</sub> epitaxial films: high throughput optimization using a temperature gradient method *Appl. Phys. Lett.* **82** 1571–3
- [25] Mitsui T and Nomura S 1981 *Landolt-Börnstein* vol 16 (Berlin: Springer) p 538
- [26] Schenck P K and Kaiser D L unpublished
- [27] Hanak J J 1970 The 'multiple-sample concept' in materials research: synthesis, compositional analysis and testing of entire multicomponent systems *J. Mater. Sci.* **5** 964
- [28] Christen H M *et al* 2003 An improved continuous compositional-spread technique based on pulsed-laser deposition and applicable to large substrate areas *Rev. Sci. Instrum.* **74** 4058–62
- [29] Fan S *et al* 1999 Self-oriented regular arrays of carbon nanotubes and their field emission properties *Science* **283** 512–4
- [30] Su M *et al* 2000 Lattice-oriented growth of single-walled carbon nanotubes *J. Phys. Chem. B* **104** 6505–8
- [31] Li W Z *et al* 1996 Large-scale synthesis of aligned carbon nanotubes *Science* **274** 1701–3
- [32] Cassell A M *et al* 1999 Large scale CVD synthesis of single-walled carbon nanotubes *J. Phys. Chem. B* **103** 6484–92
- [33] Kiang C-H *et al* 1996 Catalytic effects of heavy metals on the growth of carbon nanotubes and nanoparticles *J. Phys. Chem. Solids* **57** 35–9
- [34] Li Y *et al* 2001 Preparation of monodispersed Fe–Mo nanoparticles as the catalyst for CVD synthesis of carbon nanotubes *Chem. Mater.* **13** 1008–14
- [35] Delzeit L *et al* 2001 Multilayered metal catalysts for controlling the density of single-walled carbon nanotube growth *Chem. Phys. Lett.* **348** 368–74
- [36] Lacerda R G *et al* 2004 Growth of high-quality single-wall carbon nanotubes without amorphous carbon formation *Appl. Phys. Lett.* **84** 269–71
- [37] Liu B C *et al* 2003 Synthesis of single- and double-walled carbon nanotubes by catalytic decomposition of methane *Chem. Phys. Lett.* **373** 475–9
- [38] Christen H M *et al* Discovery and optimization of metallic catalysts for the growth of long-length forests of vertically aligned multi-walled carbon nanotubes *Nano Letters* accepted for publication